Enhanced light trapping in solar cells with a meta-mirror following generalized Snell's law

M. Ryyan Khan,[1,*] Xufeng Wang,[1] Peter Bermel,[1] and Muhammad A. Alam,[1,2]

[1]*School of Electrical and Computer Engineering, Purdue University, West Lafayette, IN 47907, USA*
[2]*alam@purdue.edu*
[*]*khan23@purdue.edu*

Abstract: As the performance of photovoltaic cells approaches the Shockley-Queisser limit, appropriate schemes are needed to minimize the losses without compromising the current performance. In this paper we propose a planar absorber-mirror light trapping structure where a conventional mirror is replaced by a meta-mirror with asymmetric light scattering properties. The meta-mirror is tailored to have reflection in asymmetric modes that stay outside the escape cone of the dielectric, hence trapping light with unit probability. Ideally, the meta-mirror can be designed to have such light trapping for any angle of incidence onto the absorber-mirror structure. We illustrate the concept by using a simple gap-plasmon meta-mirror. Even though the response of the mirror is non-ideal with the unwanted scattering modes reducing the light absorption, we observe an order of magnitude enhancement compared to single pass absorption in the absorber. The bandwidth of the enhancement can be matched with the range of wavelengths close to the solar cell absorber band-edge where improved light absorption is required.

OCIS codes: (160.3918) Metamaterials; (040.5350) Photovoltaic.

References and links

1. W. Shockley and H. J. Queisser, "Detailed Balance Limit of Efficiency of p-n Junction Solar Cells," J. Appl. Phys. **32**(3), 510 (1961).
2. X. Wang, M. R. Khan, J. L. Gray, M. A. Alam, and M. S. Lundstrom, "Design of GaAs Solar Cells Operating Close to the Shockley-Queisser Limit," IEEE J. Photovoltaics **3**(2), 737–744 (2013).
3. B. M. Kayes, H. A. Atwater, and N. S. Lewis, "Comparison of the device physics principles of planar and radial p-n junction nanorod solar cells," J. Appl. Phys. **97**(11), 114302 (2005).
4. M. M. Adachi, M. P. Anantram, and K. S. Karim, "Core-shell silicon nanowire solar cells," Sci. Rep. **3**, 1546 (2013).
5. M.-H. Hsu, P. Yu, J.-H. Huang, C.-H. Chang, C.-W. Wu, Y.-C. Cheng, and C.-W. Chu, "Balanced carrier transport in organic solar cells employing embedded indium-tin-oxide nanoelectrodes," Appl. Phys. Lett. **98**(7), 073308 (2011).
6. B. Ray, M. R. Khan, C. Black, and M. A. Alam, "Nanostructured Electrodes for Organic Solar Cells: Analysis and Design Fundamentals," IEEE. J. Photovoltaics **3**, 318–329 (2012).
7. L. Hu and G. Chen, "Analysis of Optical Absorption in Silicon Nanowire Arrays for Photovoltaic Applications," Nano Lett. **7**(11), 3249–3252 (2007).
8. Q. G. Du, C. H. Kam, H. V. Demir, H. Y. Yu, and X. W. Sun, "Broadband absorption enhancement in randomly positioned silicon nanowire arrays for solar cell applications," Opt. Lett. **36**(10), 1884–1886 (2011).
9. J. Zhu, Z. Yu, G. F. Burkhard, C.-M. Hsu, S. T. Connor, Y. Xu, Q. Wang, M. McGehee, S. Fan, and Y. Cui, "Optical Absorption Enhancement in Amorphous Silicon Nanowire and Nanocone Arrays," Nano Lett. **9**(1), 279–282 (2009).
10. S. Basu Mallick, N. P. Sergeant, M. Agrawal, J.-Y. Lee, and P. Peumans, "Coherent Light Trapping in Thin-Film Photovoltaics," MRS Bull. **36**(06), 453–460 (2011).
11. S. B. Mallick, M. Agrawal, and P. Peumans, "Optimal light trapping in ultra-thin photonic crystal crystalline silicon solar cells," Opt. Express **18**(6), 5691–5706 (2010).
12. S. Jeong, M. D. McGehee, and Y. Cui, "All-back-contact ultra-thin silicon nanocone solar cells with 13.7% power conversion efficiency," Nat Commun **4**, 2950 (2013).
13. V. Kochergin, L. Neely, C.-Y. Jao, and H. D. Robinson, "Aluminum plasmonic nanostructures for improved absorption in organic photovoltaic devices," Appl. Phys. Lett. **98**(13), 133305 (2011).

#206689 - $15.00 USD Received 18 Feb 2014; revised 28 Mar 2014; accepted 31 Mar 2014; published 23 Apr 2014

14. J. Yang, J. You, C.-C. Chen, W.-C. Hsu, H. R. Tan, X. W. Zhang, Z. Hong, and Y. Yang, "Plasmonic Polymer Tandem Solar Cell," ACS Nano **5**(8), 6210–6217 (2011).
15. X. Wang, M. R. Khan, M. Lundstrom, and P. Bermel, "Performance-limiting factors for GaAs-based single nanowire photovoltaics," Opt. Express **22**(S2), A344–A358 (2014).
16. J. N. Munday and H. A. Atwater, "Large Integrated Absorption Enhancement in Plasmonic Solar Cells by Combining Metallic Gratings and Antireflection Coatings," Nano Lett. **11**, 2195–2201 (2010).
17. H. A. Atwater and A. Polman, "Plasmonics for improved photovoltaic devices," Nat. Mater. **9**(3), 205–213 (2010).
18. Z. Yu, A. Raman, and S. Fan, "Fundamental limit of nanophotonic light trapping in solar cells," Proc. Natl. Acad. Sci. U.S.A. **107**(41), 17491–17496 (2010).
19. M. A. Green, "Enhanced evanescent mode light trapping in organic solar cells and other low index optoelectronic devices," Prog. Photovolt. Res. Appl. **19**(4), 473–477 (2011).
20. E. Yablonovitch and G. D. Cody, "Intensity enhancement in textured optical sheets for solar cells," IEEE Trans. Electron. Dev. **29**(2), 300–305 (1982).
21. E. Yablonovitch, "Statistical ray optics," J. Opt. Soc. Am. **72**(7), 899–907 (1982).
22. Z. Yu, A. Raman, and S. Fan, "Fundamental limit of light trapping in grating structures," Opt. Express **18**(S3 Suppl 3), A366–A380 (2010).
23. N. Yu, P. Genevet, M. A. Kats, F. Aieta, J.-P. Tetienne, F. Capasso, and Z. Gaburro, "Light Propagation with Phase Discontinuities: Generalized Laws of Reflection and Refraction," Science **334**(6054), 333–337 (2011).
24. N. Yu, P. Genevet, F. Aieta, M. A. Kats, R. Blanchard, G. Aoust, J.-P. Tetienne, Z. Gaburro, and F. Capasso, "Flat Optics: Controlling Wavefronts With Optical Antenna Metasurfaces," IEEE J. Sel. Top. Quantum Electron. **19**(3), 4700423 (2013).
25. X. Ni, N. K. Emani, A. V. Kildishev, A. Boltasseva, and V. M. Shalaev, "Broadband Light Bending with Plasmonic Nanoantennas," Science **335**(6067), 427 (2012).
26. A. V. Kildishev, A. Boltasseva, and V. M. Shalaev, "Planar Photonics with Metasurfaces," Science **339**(6125), 1232009 (2013).
27. S. Sun, K.-Y. Yang, C.-M. Wang, T.-K. Juan, W. T. Chen, C. Y. Liao, Q. He, S. Xiao, W.-T. Kung, G.-Y. Guo, L. Zhou, and D. P. Tsai, "High-Efficiency Broadband Anomalous Reflection by Gradient Meta-Surfaces," Nano Lett. **12**(12), 6223–6229 (2012).
28. S. Sun, Q. He, S. Xiao, Q. Xu, X. Li, and L. Zhou, "Gradient-index meta-surfaces as a bridge linking propagating waves and surface waves," Nat. Mater. **11**(5), 426–431 (2012).
29. A. Pors, O. Albrektsen, I. P. Radko, and S. I. Bozhevolnyi, "Gap plasmon-based metasurfaces for total control of reflected light," Sci. Rep. **3**, 2155 (2013).
30. Y. Luo, R. Zhao, A. I. Fernandez-Dominguez, S. A. Maier, and J. B. Pendry, "Harvesting light with transformation optics," Sci. China Inf. Sci. **56**(12), 1–13 (2013).
31. S. Larouche and D. R. Smith, "Reconciliation of generalized refraction with diffraction theory," Opt. Lett. **37**(12), 2391–2393 (2012).
32. V. Liu and S. Fan, "S4 : A free electromagnetic solver for layered periodic structures," Comput. Phys. Commun. **183**(10), 2233–2244 (2012).
33. A. F. Oskooi, D. Roundy, M. Ibanescu, P. Bermel, J. D. Joannopoulos, and S. G. Johnson, "Meep: A flexible free-software package for electromagnetic simulations by the FDTD method," Comput. Phys. Commun. **181**(3), 687–702 (2010).

1 Introduction and background

The photovoltaic (PV) devices converts sunlight to electricity in two steps: sunlight is absorbed to create electron-hole pairs within the active layer, and the photo-generated carriers are extracted by the built-in electric field of the device. As solar cell technologies move closer toward the ideal thermodynamic (Shockley-Queisser, S-Q) limit of PV performance [1], the new designs need to be more effective in reducing the remaining loss components without introducing new ones [2]. Unfortunately, non-ideal material characteristics couple absorption-transport processes in a fundamental way: the finite optical absorption sets the minimum (optical) thickness of the absorber (optical thickness), while finite mobility and radiative/non-radiative recombination set the maximum (electrical) thickness limit of the cell.

The strategies that address the issue of absorption or carrier extraction all rely on decoupling optical and electrical thicknesses of solar cells. For example, solar cell configurations such as radial junction nanowire (NW) PV [3,4], and projected electrodes [5,6] focus on decoupling the light absorption from the carrier extraction length by absorbing light vertically, but separating the carrier laterally. These structures provide a shorter and more efficient path for carrier collection. Light trapping (LT) schemes instead focus on collecting the carrier vertically so that electrical path-length is reduced, while reducing reflection and

#206689 - $15.00 USD Received 18 Feb 2014; revised 28 Mar 2014; accepted 31 Mar 2014; published 23 Apr 2014

increasing lateral scattering of the light so that optical absorption is enhanced. We can subdivide the LT schemes in two broad categories: (i) nano-structuring the active layer itself, and (ii) redesigning the dielectric environment around it. In the first category, random texturing, NW array, nanocone (NC) structures [7–9] reduce reflection of the incoming light and induce scattering for overall improved absorption. Other photonic crystal structures can scatter light inside the dielectric and yield longer light passage in the absorber [10–12]. Also, embedded plasmonic nano-particles [13,14] can create localized high fields which in turn greatly enhance localized absorption. Unfortunately, these strategies also increase the surface area for recombination and the corresponding degradation in charge collection may ultimately negate any gain from light trapping [15].

In the second category, a separate dielectric or metallic scatterer layer is used to enhance absorption of the incident light inside the un-patterned, planar absorber layer. These approaches include scattering of light from metal particles at the top surface, or generation of surface plasmon polaritons (SPPs) at the back metal grating [16,17]. However, at optical frequencies, typical plasmonic materials absorb a fraction of the incident photons, introducing an additional loss mechanism in the device. The patterning could also be done in a separate lossless dielectric to scatter the light going into the absorber. These designs aim at scattering light into higher angles to enhance the light path yielding good absorption [18,19]. The key idea here is to couple the normally incident light into guided modes. However, the lossless patterned dielectric scatterers usually have complex designs and could be challenging to implement in practice.

In this paper, we wish to explore the potential of a new approach to dielectric light scattering into lateral guided modes by meta-mirrors. Remarkably, even a nominal design improves light absorption by an order of magnitude. Note that, absorption enhancement limits have been discussed for both geometric [20,21] and wave optics regime [22]. Yablonovitch *et al*. [20,21] showed that absorption in a weak absorber can be enhanced up to a factor of $4n^2$. Our proposed concept suggests that these limits may be exceeded (and the light may be trapped with unit probability) by using a meta-mirror as a back reflector, although the specific mirror design that achieves this perfect absorption is yet to be determined.

Briefly, recent developments in the concepts of meta-surface [23–29] have shown the possibility of rearranging light propagation in planar structures. In this work, we propose inserting a reflecting meta-mirror at the back of the solar cell to asymmetrically scatter the rays. The asymmetric scattering follows the generalized Snell's law of reflection [23]. In principle, the meta-mirror can be designed to scatter light primarily into a single mode that stays away from the critical angle of the front surface; and thereby ensuring total internal reflection (TIR). As we show in Sec. 2, an idealized meta-mirror that scatters the light into such *single* mode has the potential to perfectly trap the entire incident light irrespective of the dielectric thickness (i.e., both in geometric or wave optics regime) for any angle of incidence. In practice, exclusive scattering into a single mode may not be possible. Also, a solar cell is a broadband absorber (although absorption close to the band-edge is most critical), and, therefore, wavelength dependence of asymmetric scattering associated the practical design must be explored. Despite these issues, a nominal design discussed in Sec. 3 anticipates an order of magnitude improvement over single pass absorption. We conclude by suggesting that an optimized structure has the potential for considerably higher enhancement of optical light trapping and the bandwidth is always sufficiently large for the scheme to be a practical light trapping scheme for high efficiency solar cells working close to the S-Q limit.

2 Theory and design of meta-mirrors

2.1 Theory of perfect absorption

Consider an optical 'mirror' which adds a phase shift $\Phi(x)$ at any point x on the mirror surface upon each reflection of the incident wave. In the special case when $\Phi(x)$ varies

#206689 - $15.00 USD Received 18 Feb 2014; revised 28 Mar 2014; accepted 31 Mar 2014; published 23 Apr 2014

linearly with x, we have $\Delta k_x = d\Phi(x)/dx =$ constant. This can be viewed as an addition of constant tangential k-component Δk_x to the incident plane wave, i.e.,

$$k_{x(r)} = k_{x(i)} + \Delta k_x. \tag{1}$$

Here, $k_{x(i)}$ and $k_{x(r)}$ are the x-components of the wave vectors of the incident and reflected plane waves, respectively. The plane wave is assumed to be in xz-plane in a dielectric with refractive index n. Equation (1) states that a plane wave propagating in a dielectric will not be reflected with an angle equal to the incidence angle expected from the conventional Snell's Law of reflection. We can rewrite the previous relationship as follows,

$$k_0 n \sin\theta_r = k_0 n \sin\theta_i + \Delta k_x \tag{2}$$

$$\text{or, } \theta_r = \sin^{-1}\left(\sin\theta_i + \frac{\Delta k_x}{k_0 n}\right) = \sin^{-1}\left(\sin\theta_i + \delta\right) \tag{3}$$

Here, $\theta_i = 0$ and θ_r are the incidence and reflected angles of the plane wave at the *mirror surface*. k_0 is the free-space wave vector at wavelength of interest λ_0. The mirror effectively steers the incident plane wave into higher angles breaking the conventional rule of specular reflection in planar mirrors. And, for $\sin\theta_i \geq (1-\delta)$ the scattered waves become surface waves confined close to the mirror dielectric interface. This causes asymmetric scattering, which can be referred to as the 'generalized Snell's law' of reflection. We will show in the following discussions how this asymmetric scattering property of the mirror can be ideally used to develop a scheme for perfect light trapping.

Figure 1(a) shows a light trapping scheme in a dielectric. Assume that the mirror follows generalized Snell's law of reflection. Light incident from air refracts into the dielectric with some angle θ_{i1} inside the escape cone (see Fig. 1(b)). Thus we have $|\theta_{i1}| < \theta_C$ (here $\theta_C = \sin^{-1}(1/n)$ is the critical angle of refraction). Then the plane wave hits the back mirror and reflects back with a larger angle, θ_{r1} as expected from Eq. (3). The mirror is designed under the constraint that, for any $|\theta_{i1}| < \theta_C$, the reflected wave assumes an angle $\theta_{r1} > \theta_C$. Thus, the light reflected from the mirror will reach the top dielectric-air interface with angle greater than θ_C —resulting in total internal reflection. The plane wave will travel back to the mirror with new incidence angle of $\theta_{i2} = \theta_{r1}$. Now, the reflected wave will have $\theta_{r2} > \theta_{i2}$, i.e., $\theta_{r2} > \theta_{r1} > \theta_C$. This cycle will continue with the light attaining a higher angle after each bounce off the back mirror. Rays with larger angle of propagation will always stay outside the escape cone and remain trapped inside the dielectric. Note that, after some N bounce cycles, the incident angle on the mirror will be $\theta_{iN} \geq \sin^{-1}(1-\delta)$. In this case, instead of reflecting back into a propagating mode, the light wave will scatter into a surface wave along the dielectric-mirror interface.

The scheme provides means for trapping the incident light indefinitely—a dielectric with the smallest of absorption coefficient will have perfect absorption. Ideally, the structure absorbs 100% of the light, irrespective of how weak the absorption coefficient may be. Thus, the conceptual structure can have an absorption enhancement factor limited only by the inverse of the original optical absorption — for poor absorbers, this breaks the conventional absorption enhancement limit (e.g., the Yablonovitch $4n^2$ limit [20,21]). This perfect absorption should not be misunderstood to be unphysical, because detailed balance ensures

#206689 - $15.00 USD Received 18 Feb 2014; revised 28 Mar 2014; accepted 31 Mar 2014; published 23 Apr 2014

that at open circuit condition, absorption is counterbalanced by appropriately high radiation [30].

Figure 1 shows an example of the path followed by light ray inside the dielectric ($n = 3.5$) of the proposed structure. Here, for the ray tracing calculations, we have assumed $\delta = \sin\theta_C$.

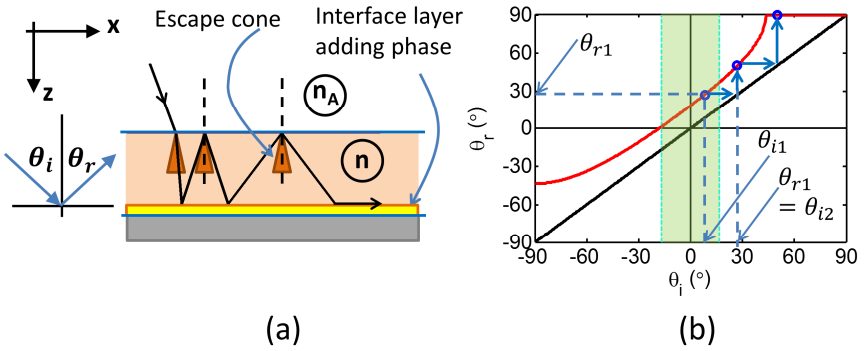

Fig. 1. (a) The concept of light trapping is shown. A dielectric with refractive index n is placed on top of a meta-mirror which follows the generalized Snell's law of reflection. The meta-mirror is shown here as a combination of a perfect mirror and a gradient phase adding interface layer. The ideal path for the light ray is shown. (b) The red line shows the law of reflection at the back meta-mirror. The black line represents specular reflection for total internal reflection at the top dielectric-air interface. The shaded region represents the escape cone angles. The blue circles are the incident angles at the meta-mirror after multiple bounces for the example illustrated in (a).

2.2 Design rules for meta-mirror

Phases are only defined per modulo 2π , i.e., the added phase of $\Phi(x)$ has the same effect as the added phase of $\Phi(x)+m2\pi$, where m is an integer. Therefore, we can wrap the linear profile of $\Phi(x)$ into a periodic triangular form, where the added phase varies linearly from 0 to 2π inside a period. This profile of $\Phi(x)$ for the mirror can be created by an extra graded index dielectric on top of a conventional mirror [31] or by a meta-surface [23,27] [29].

The period Γ_x of the mirror structure depends on the required slope of $\Phi(x)$. Hence Γ_x will be determined by $\Delta k_x = d\Phi(x)/dx$ (or, equivalently by $\delta = \Delta k_x / k_0 n$). As explained earlier, for the light trapping scheme to work, the value of δ is constrained by θ_C at a given wavelength $\lambda_0 = k_0 / 2\pi$. Thus the mirror structure period should be limited by constraints set by θ_C , or equivalently by the refractive index n of the active layer dielectric and the wavelength λ_0 . However, as we will show in the following analysis, design of Γ_x only depends on the wavelength of interest.

As explained earlier, the light rays initially reach the mirror at an angle of $(-\theta_C) < \theta_{i1} < \theta_C$. To ensure the design works for all incident angles, we start with the worst-case scenario, i.e., $\theta_{i1} = -\theta_C$. And, we require that $\theta_{r1} \geq \theta_C$. Thus from Eq. (3), we have:

$$\begin{aligned} &\sin\theta_{r1} = \sin\theta_{i1} + \delta \geq \sin\theta_C \\ \text{or, } &-\sin\theta_C + \delta \geq \sin\theta_C \\ \text{or, } &\delta \geq 2\sin\theta_C \end{aligned} \tag{4}$$

#206689 - $15.00 USD Received 18 Feb 2014; revised 28 Mar 2014; accepted 31 Mar 2014; published 23 Apr 2014

Therefore, we need to choose at least $\delta = 2\sin\theta_C = 2/n$. Now, the period is related to Δk_x by: $\Delta k_x = d\Phi(x)/dx = 2\pi/\Gamma_x$. Thus the period for the mirror design is found as follows:

$$\Gamma_x = \frac{2\pi}{\Delta k_x} = \frac{2\pi}{k_0 n\delta} \le \frac{\lambda_0}{2}$$

The above mentioned condition is sufficient to trap light inside the planar dielectric (or absorber) for any incidence angle from air. If we focus on normal incidence, i.e., $\theta_{i1} = 0$ then the design condition is relaxed to $\Gamma_x \le \lambda_0$. We will consider only normal incidence for the design studies presented in this paper. Note that, wavelengths away from λ_0 may be scattered into multiple modes. However, for a range of wavelengths (λ) close to λ_0, most of the scattered wave will couple into the intended mode following the generalized Snell's law. Of-course, for short-wavelengths $\lambda < \Gamma_x$ we will have $\theta_{r1} < \theta_C$ and thus there will be no light trapping for such wavelengths. The bandwidth for this response depends on the specifics of the design. The concept of a periodic meta-mirror is most simply illustrated by a graded refractive index layer on top of a conventional mirror (see Appendix A).

While the periodic meta-mirror based on graded index layer explains the basic concepts of asymmetric scattering intuitively, in practice it is easier to design equivalent meta-mirror based on the concept of 'gap-plasmon' meta-surface [29], discussed as follows.

3 Gap-plasmon based periodic meta-mirrors

3.1 Properties of designed meta-mirror

Figure 2(a) shows a gap-plasmon meta-surface mirror embedded in a dielectric ($n = 3.5$). The various metal strip-sizes in gap-plasmon configuration add gradient phase $\Phi(x)$ ranging from 0 to 2π. The details of the meta-mirror design are given in Appendix B. The numerical calculations are done using S^4 [32], which is based on Rigorous Coupled Wave Analysis (RCWA). Metal components have been assumed to be loss-less having refractive index of $n_{metal} = 7i$. It is also taken as non-dispersive for clear demonstration of the concept. The stability of the results has been checked by testing for higher number of Fourier components. Since RCWA does not automatically yield reliable results for metal inclusions in the structure, we validated the results by using Finite Difference Time Domain (FDTD) simulations in Meep [33] as well. We choose period $\Gamma_x = 550\,\text{nm}$ for the design wavelength $\lambda_0 = 600\,\text{nm}$. The structure is uniform along y-direction. And, we only consider H_y-polarization for the incident light. Our design will only focus on one polarization to provide a clear illustration and simple explanation of the design idea. However, it is possible to design a meta-mirror to simultaneously address both polarizations, as explained in Ref [29].

The transfer characteristics (θ_r vs. θ_i) of the mirror is presented in Fig. 2(c) as a spectrum of scattered H_y field components. The (+ 1)-diffraction mode (also marked in the figure) corresponds to the generalized Snell's law of reflection, Eq. (3). The angle of reflection for normal incidence $\theta_i = 0$ can be calculated for the (+ 1)-diffraction mode as follows:

$$\theta_r^{(+1)} = \sin^{-1}(\delta) = \sin^{-1}\left(\frac{\Delta k_x}{nk}\right) = \sin^{-1}\left(\frac{2\pi/\Gamma_x}{n2\pi/\lambda}\right) = \sin^{-1}\left(\frac{\lambda/n}{\Gamma_x}\right). \qquad (5)$$

For $\lambda = 600\,\text{nm}$, $\Gamma_x = 550\,\text{nm}$, and $n = 3.5$, we find $\theta_r^{(+1)} = 18.16^\circ$ which matches with the numerical simulations.

#206689 - $15.00 USD Received 18 Feb 2014; revised 28 Mar 2014; accepted 31 Mar 2014; published 23 Apr 2014

Although the (+ 1)-diffraction mode represents the desired $\theta_i - \theta_r$ relationship of the 'generalized Snell's law of reflection', Fig. 2(c) shows that there are other scattered modes as well. This set of parasitic couplings can only contribute to some specific modes as a consequence of the periodicity of the mirror. For example, for $\theta_i = 0$, the scattered angle is expected to assume a value $\theta_r = \sin^{-1}(m\Delta k_x / nk) = \sin^{-1}(m\lambda / n\Gamma_x)$ for any structure with period Γ_x, where the order of the modes are given by $m = 0, \pm 1, \pm 2, \ldots$, etc. However, a linear phase profile $\Phi(x)$ created by the sub-cells can ensure exclusive coupling into $m = +1$ mode. Although only $m = +1$ is desired here, some amplitude contribution in other modes cannot be avoided because of the non-linear phase profile of 'sub-cells' in one period (details about sub-cells are in Appendix B), and finite mutual coupling between adjacent sub-cells. This is especially prominent at higher angles of incidence θ_i on the meta-mirror. For example, as presented in Fig. 2(b), the scattered wave for normal incidence (top profile) at $\lambda = 600$nm show minimum distortion in the plane wave. However, as the angle of incidence increases (e.g., $\theta_i = 15^\circ$), we start to see perturbation in the scattered field profile (middle profile) due to contribution of the unwanted modes. The existence of these parasitic modes degrades light trapping, as they allow the light to exit through the escape cone.

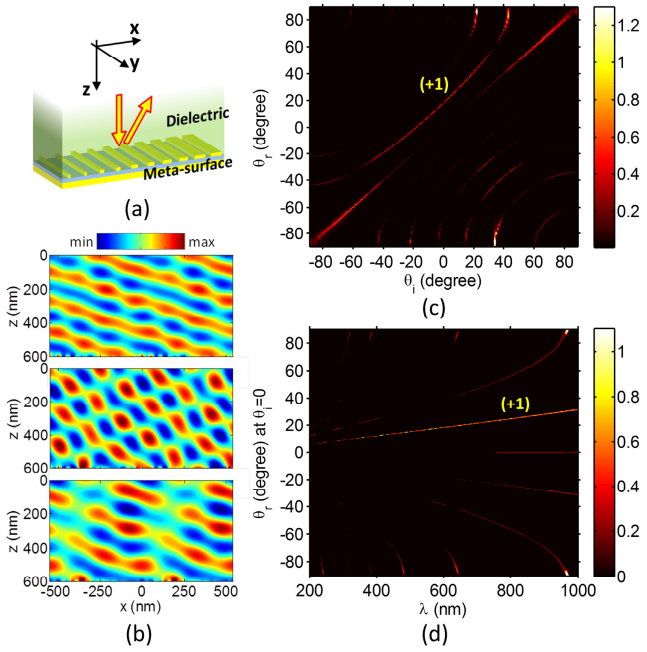

Fig. 2. (a) The meta-surface mirror configuration embedded in the dielectric. (b) Scattered H_y field profile for: (top) $\theta_i = 0, \lambda = 600$nm, (middle) $\theta_i = 15^\circ, \lambda = 600$nm, and (bottom) $\theta_i = 0, \lambda = 700$nm. (c) The transfer characteristics (θ_r vs. θ_i) are shown as a spectrum of scattered H_y field amplitudes at $\lambda = 600$ nm. (d) The scattered H_y field amplitudes for different θ_r as a function of λ is shown (at $\theta_i = 0$). Here, the mode marked (+ 1) corresponds to the generalized Snell's law of reflection.

#206689 - $15.00 USD Received 18 Feb 2014; revised 28 Mar 2014; accepted 31 Mar 2014; published 23 Apr 2014

Note that the $\theta_i - \theta_r$ relationship shown in Fig. 2(c) predominantly follows the generalized Snell's law of reflection for low θ_i (i.e., $|\theta_i| < 20^\circ$). However, larger θ_i reverts to Snell's Law, i.e., specular reflection (with small contribution from other diffraction modes). For this specific structure, no surface wave is observed for the high incidence angles—this is a deviation from the ideal characteristics. A meta-mirror using a 'xylophone'-like gap-plasmon configuration, as in [27], is likely to show much improved characteristics.

Also Eq. (5) predicts that $\theta_r^{(+1)}$ would increase with λ. This is seen in Fig. 2(d). The reflection angle θ_r is presented as a function of λ (at $\theta_i = 0$). Note that for $\lambda < \Gamma_x$, from Eq. (5) we have $\theta_r^{(+1)} < \theta_C$. As explained earlier in Sec. 2.1, the situation mentioned above breaks the condition for our light trapping scheme. The higher wavelengths gradually allow more contributions from modes other than $m = +1$ — this is reflected in the perturbed scattered field shown in Fig. 2(b) (bottom profile). Also, note that the larger contribution for the $\theta_r = 0$ mode is observed for $\lambda > 800$ nm. This means that the meta-mirror is deviating from the generalized Snell's law and showing more specular reflection outside the aforementioned wavelength range. This indicates that light trapping may be degraded for $\lambda > 800$ nm for the structure built using this meta-mirror. We will address the issue further in the following discussions.

3.2 Light-trapping in planar dielectric with back meta-mirror

Next let us calculate the light trapping using the proposed scheme. As we have discussed, the gap-plasmon periodic meta-mirror design proposed here is not ideal: (i) there is scattering into modes other than the desired mode, (ii) surface waves are not generated, and (iii) there is considerable angle and wavelength dependence of the mirror response.

For the study of absorption, let us choose the absorber thickness $L = 500$ nm (which would be typical for thin film solar cell) on top of the mirror. To reduce reflections off the top surface, a quarter wave matched (for $\lambda_0 = 600$ nm) layer is used as an ARC. We choose refractive index $n = 3.5$ and absorption coefficient $\alpha = 10^5$ /m. Both n and α are assumed to be non-dispersive in the wavelength range of interest ($200\text{nm} < \lambda < 1000\text{nm}$) for better comparison of the light trapping properties. Note that the dielectric and metal in the meta-surface structure are also assumed to be non-dispersive.

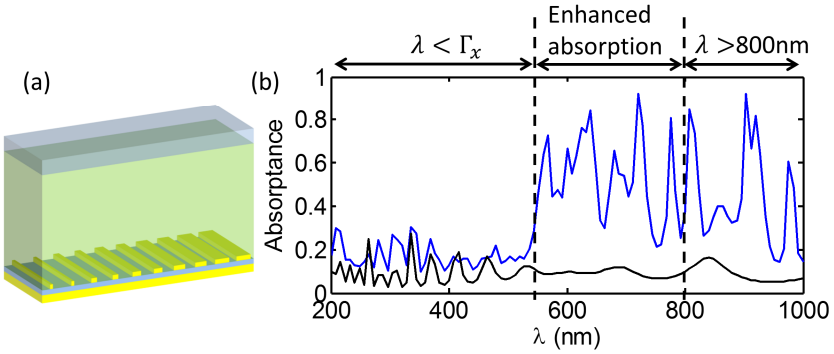

Fig. 3. (a) The light trapping scheme for thin film solar cell is shown using the meta-surface mirror. (b) The black line represents the absorption in the structure with a conventional mirror at the back. The blue line in (b) shows the absorption in the absorber layer for structures in (a).

The blue line in Fig. 3(b) represents the absorptance in the structure constructed using the meta-mirror configuration at the back (as shown in Fig. 3(a)). The black line shows the

#206689 - $15.00 USD Received 18 Feb 2014; revised 28 Mar 2014; accepted 31 Mar 2014; published 23 Apr 2014

absorption in the same cell structure only with a conventional mirror at the back. As expected, the absorption in the planar cell is $\approx 2\alpha L = 0.1$ (black line). For the meta-mirror configuration in Fig. 3(b), there is minimal change in absorptance for $\lambda < \Gamma_x = 550$ nm as the design constraint is not satisfied in this wavelength range. Also, note that, the absorption starts to go down for $\lambda > 800$ nm as predicted from the previously studied mirror properties. It is clear that there is an average absorption enhancement of a factor of ~5.75, compared to the conventional back mirror structure, for $550\text{nm} < \lambda < 800\text{nm}$. Obviously, the band of wavelengths where the absorption enhancement occurs can be shifted to arbitrary wavelengths by tailoring the meta-mirrors at appropriate periodicities. The study considered here only focuses on normally incident light. This reflects the operating conditions for solar cells with dual-axis tracking that could experience direct normal incidence throughout the day. Of course, a meta-mirror designed using $\Gamma_x \le \lambda_0 / 2$ can ideally trap light for all angles of incidence (see Sec. 2.2 for details).

Although the solar cell is a broadband absorber, the finite bandwidth over which a meta-mirror sustains significant gain is not a concern. For a practical solar cell (e.g., Si), the absorption is strong for high energy photons (lower wavelengths) away from the band-edge. Thus, almost all the high energy photons are absorbed within practical cell thickness—the light trapping schemes are irrelevant. However, the absorption coefficients close to the band-edge are considerably lower and it is within this narrow bandwidth where light-trapping is relevant and important. So long as the meta-surface mirrors are designed to overlap this weak absorption regime, the improvement in light trapping can be significant. Also, the proposed scheme is expected to be fairly insensitive to small changes in the optical real refractive index for practical PV materials.

Finally, we realize that the meta-mirror structure proposed here consists of sub-wavelength components that may be difficult to fabricate. Despite the difficulty, however, recent works presented in Refs [25,27,29]. show that such structures are feasible and can be demonstrated experimentally.

4. Conclusions

In this paper, we have proposed a planar structure for light trapping which utilizes the asymmetric scattering of the meta-mirror at the back. The meta-mirror only reflects light into a single mode following generalized Snell's law of reflection. The ideal configuration anticipates perfect absorption for all angles of incidence onto the planar absorber. Practical implementation based on gap-plasmon meta-mirrors may inherently allow scattering light into multiple diffraction modes. The undesired modes cause the light to leak out of the structures. Although perfect absorption is no longer expected, an optimized design can lower coupling to unwanted modes and improve overall absorption considerably. Indeed, a nominal design presented here shows an absorption gain of a factor of ~11.5 compared to single pass absorption in the dielectric (i.e., factor of ~5.75 compared to a back mirrored planar structure). Obviously, the gap-plasmon meta-mirror is just one example of a meta-surface being capable of scattering light asymmetrically. It remains an important open question to see if other implementations might provide improved absorption approaching the ideal limit.

Appendices

Appendix A. Graded index mirror

For a more qualitative understanding, let us consider a hypothetical mirror which can demonstrate the properties discussed in Sec.2.1. The simplest of examples for this purpose would be a graded refractive index layer on top of a conventional mirror (see Fig. 4(a)). Each segment has the same thickness, but different refractive index, and therefore, provides varying optical paths for the incoming wave. The phase added to the light wave by the

#206689 - $15.00 USD Received 18 Feb 2014; revised 28 Mar 2014; accepted 31 Mar 2014; published 23 Apr 2014

segments will follow the index gradient; therefore, as the wave reflects from the graded index layer, it will accumulate a spatially gradient phase $\Phi(x)$. The graded index layer has periodic and linearly varying indices ranging from n_L to n_H. For a large number of sub-segments, if the phase added by the dielectric with index n_L is Φ_L then the phase added by segment n_H would be $\Phi_L + 2\pi$.

Let us assume that every period consists of N_S segments and the refractive index changes by Δn between consecutive segments. The phase added at the end of each period is 2π, or equivalently, the extra optical path length would be λ_0 (design wavelength). Thus, for the graded index layer of thickness t_{GI},

$$\left(\Delta n\, N_S\right) \times t_{GI} \times 2 = \lambda_0. \tag{6}$$

Here, $\Delta n\, N_S$ corresponds to the refractive index variation over one period. The factor of two is due to the fact that the light travels through the layer twice as there is a mirror at the back. Finally, we can write:

$$\Delta n = \frac{\lambda_0}{2t_{GI}} \times \frac{1}{N_S}, \tag{7}$$

$$n_{GI} = n_L + \beta \Delta n. \tag{8}$$

The refractive indices of the graded index layer sub-segments are given by n_{GI} in the above equation; where, $\beta = 0, 1, 2, \ldots, \left(N_S - 1\right)$.

Figure 4(a) shows the graded index mirror embedded in a dielectric ($n = 3.5$). We introduce a matching layer on top of the graded index layer to minimize specular reflection. We choose period $\Gamma_x = 550$ nm for the design wavelength $\lambda_0 = 600$ nm (as mentioned in Sec. 2.2, the light trapping scheme requires that $\Gamma_x < \lambda_0$). The structure is uniform along y-direction. The design parameters are summarized in Table 1. We only consider H_y-polarization for the incident light.

The transfer characteristics (θ_r vs. θ_i) of the mirror is presented in Fig. 4(b). The $\theta_i - \theta_r$ relationship predominantly follows the generalized Snell's law of reflection for low θ_i (i.e., $\left|\theta_i\right| < 20^\circ$). However, larger θ_i reverts to Snell's Law, i.e., specular reflection (with small contribution from other diffraction modes). No surface wave is observed for the high incidence angles. These characteristics are similar to those of the meta-mirror discussed in Sec.3.1. Note that we have $\theta_r^{(+1)} = 18.16^\circ$ for this structure as well.

Figure 4(c) shows the $\theta_r - \lambda$ properties (at $\theta_i = 0$). We see that $\theta_r^{(+1)} < \theta_C$ for $\lambda < \Gamma_x$ which does not support the light trapping constraint for our proposed scheme. Also, observe that a more prominent mode emerges at $\theta_r = 0$ for $\lambda > 800$ nm—similar to the meta-mirror structure.

#206689 - $15.00 USD Received 18 Feb 2014; revised 28 Mar 2014; accepted 31 Mar 2014; published 23 Apr 2014

Table 1. Design parameters for the graded index mirror structure.

Parameter	Value / expressions
λ_0	600 nm
Γ_x	550 nm
n_L	$=1.5\times n$
t_{GI}	$=\frac{1}{n_L}\times\frac{7\lambda_0}{4}\times\frac{1}{2}$
N_S	5
Δn	$=\frac{\lambda_0}{2t_{GI}}\times\frac{1}{N_S}$
$n_{matching}$	$=\sqrt{n_L\, n}$
$t_{matching}$	$=\frac{1}{n_{matching}}\times\frac{5\lambda_0}{4}$

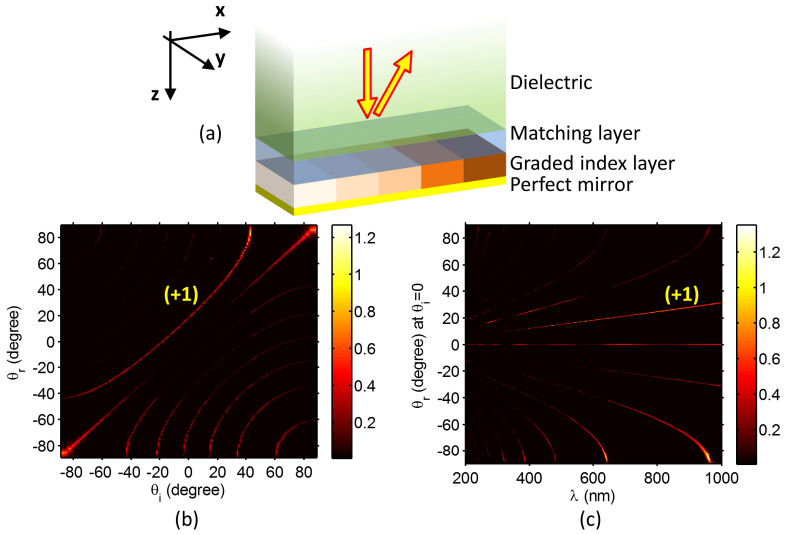

Fig. 4. (a) The graded index mirror configuration embedded in the dielectric. (b) The transfer characteristics (θ_r vs. θ_i) are shown as a spectrum of scattered H_y field amplitudes at $\lambda = 600$ nm. (c) The scattered H_y field amplitudes for different θ_r as a function of λ is shown (at $\theta_i = 0$). Here, the mode marked (+ 1) corresponds to the generalized Snell's law of reflection.

The absorption enhancement using the graded index mirror is presented here for absorber thickness of $L = 500$ nm, and absorption coefficient of $\alpha = 10^5$ /m. The study is similar to the

#206689 - $15.00 USD Received 18 Feb 2014; revised 28 Mar 2014; accepted 31 Mar 2014; published 23 Apr 2014

one done for the meta-mirror configuration (in Sec.3.1) for $200\text{nm} < \lambda < 1000\text{nm}$. The absorption in the structure shown in Fig. 5(a) is represented by the blue line in Fig. 5(b). The black line is the absorption in a structure having a conventional mirror at the back. As expected, the enhancement of absorptance is minimal for $\lambda < \Gamma_x = 550$ nm (also see Sec.2.2). However, absorption peaks are observed in this λ-range. This can be associated with the resonances created by the series of dielectric layers.

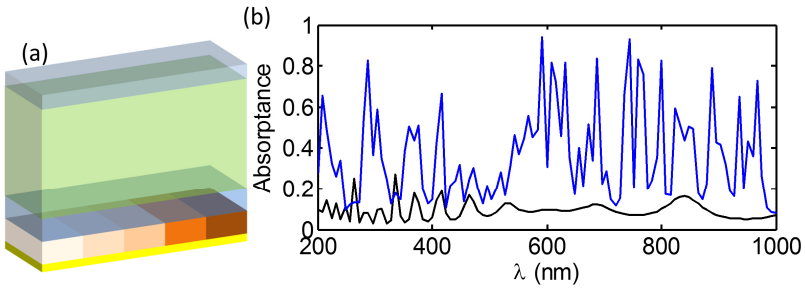

Fig. 5. (a) The light trapping scheme for thin film solar cell is shown using the graded index mirror. The ARC layer on top of the dielectric is used to minimize reflection of the incident light. (b) The black line shows the absorption in the structure with a conventional mirror at the back. The blue line show the absorption in the absorber layer for structures in (a).

Appendix B. Design of gap-plasmon periodic meta-mirror

The meta-mirror has a periodic structure. Each period, i.e., the supercell, is constructed from 10 sub-cells, see Fig. 6(a). Each sub-cell is intended to add increasing phases to get $\Phi(x)$ of 0 to 2π within each period. We design the meta-mirror as a 'gap-plasmon' meta-surface structure [27,29]. A dielectric material (refractive index 1.38) is placed between a metal strip of width W and a metal plate. The thicknesses of these layers are marked in Fig. 6(a). Varying W will add different phases to the scattered (reflected) wave. Of-course this response has to be investigated inside the dielectric (active layer of the device) with $n = 3.5$. The metal for the numerical studies is assumed to be loss-less and non-dispersive with refractive index $n_{metal} = 7i$ (i.e., relative permittivity of –49). The phases added to the reflected waves under such constraints are presented in Fig. 6(b) as a function of W.

The design is done under normal incidence condition (blue solid line in Fig. 6(b)). Now, 10 sub-cells that add $\beta \times 36^\circ$ phases (here $\beta = 0,1,\ldots,9$) need to be used to construct the supercell. The period of the sub-cell is $\Gamma_{x-sub} = 55\text{nm}$; thus period of the meta-mirror is $\Gamma_x = 10 \times \Gamma_{x-sub} = 550\text{nm}$. The widths (W) of individual stripes are tabulated in Fig. 6. Note that, as the change in phase added Φ spans from 0° to $\sim 300^\circ$ for W range of 0 to 55nm, the sub-cells do not contribute to the overall phase equally, see Fig. 6(b). This non-uniform contribution to the overall phase, however, has only a minor effect on the meta-mirror performance for normally incident light. These simulations were done using S^4 [32] as explained in Sec.3.1.

The supercell constructed from the selected sub-cells (as tabulated in bottom of Fig. 6) is expected to show a spatially linear phase profile. It is presented in Fig. 6(c) as a variation in the relative phases. It is clear that, for normal incidence $(\theta_i = 0)$ onto the meta-mirror, a linear phase profile is preserved (the red circles). However, the linear phase profile is not observed for oblique incidence (blue crosses, $\theta_i = 40^\circ$). The disturbance of the linear phase profile for oblique incidence causes the $\theta_i - \theta_r$ characteristics to stray from the generalized Snell's law of reflection.

#206689 - $15.00 USD Received 18 Feb 2014; revised 28 Mar 2014; accepted 31 Mar 2014; published 23 Apr 2014

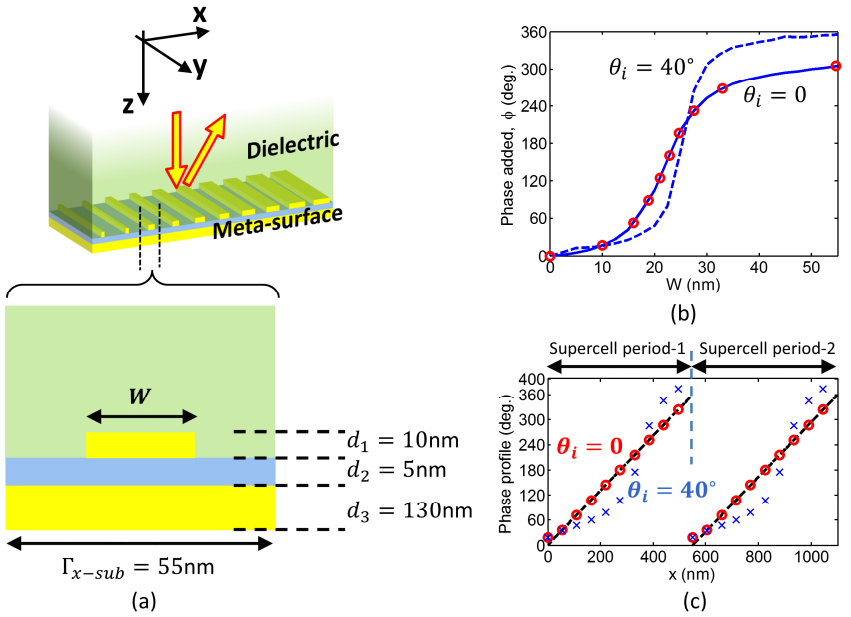

W (nm)	0	10	16.05	18.88	21.09	22.84	24.74	27.56	33.04	55
Φ (deg.)	0	16.64	52.64	88.64	124.64	160.64	196.64	232.64	268.64	305.2

Fig. 6. (a) Sub-cell of the meta-mirror periodic structure. The various lengths have been defined here. Varying metal strip widths W are used to form the supercell (single period) of the meta-mirror. (b) The phase added by super-cells as a function of W at normal incidence (blue solid line). 10 components/sub-cells are used in a supercell (red circles). These components have W values as listed in the table (bottom). (c) The 10 sub-cells create a linearly varying (relative) phase profile for normal incidence ($\theta_i = 0$), which is shown for two periods as red circles. However, for $\theta_i = 40^\circ$, the linearity of the phase profile is disrupted (see blue crosses).

Acknowledgments

The authors thank Prof. V. Shalaev and Prof. A. Boltasseva for valuable discussions. This material is based upon work supported as part of the Center for Re-Defining Photovoltaic Efficiency Through Molecule Scale Control, an Energy Frontier Research Center funded by the U.S. Department of Energy, Office of Science, Office of Basic Energy Sciences under Award Number DE-SC0001085. The computational resources for this work were provided by the Network of Computational Nanotechnology under NSF Award EEC-0228390. This was also supported by the Bay Area PV Consortium, a Department of Energy project with Prime Award number DE-EE0004946.